J|A|C|S ARTICLES

Published on Web 02/11/2010

Dynamics of 1,3-Dipolar Cycloadditions: Energy Partitioning of Reactants and Quantitation of Synchronicity

Lai Xu,[†] Charles E. Doubleday,*[,‡] and K. N. Houk*[,†]

Department of Chemistry and Biochemistry, University of California, Los Angeles, California, 90095-1569, and Department of Chemistry, Columbia University, New York, New York, 10027

Received November 4, 2009; E-mail: ced3@columbia.edu; houk@chem.ucla.edu

Abstract: The dynamics of 1,3-dipolar cycloadditions of nine 1,3-dipoles with ethylene and acetylene have been explored by quasiclassical trajectory and single trajectory calculations in the retro-cycloaddition direction to compute energy partitioning of reactants among relative translation, vibration, and rotation. The results are interpreted with an expanded version of Polanyi's Rules for bimolecular reactions, and three trends are evident. (1) Relative translation of reactants is the main contributor to surmounting the barrier, since all transition states (TSs) are early with respect to σ bond formation. (2) Vibrational excitation in the 1,3-dipole bending modes required for reaction is related to the lateness of the TS with respect to dipole bending: diazonium betaines (late TS, dipole bending required) > nitrilium betaines > azomethine betaines (early TS, dipole bending least important). This is also the order of the activation barriers (high → low). (3) The previously reported linear correlation between activation barriers and the energy required to distort reactants to their TS geometries are understandable in terms of the requirements for vibrational excitation computed here. For the 1,3-dipolar cycloadditions, single trajectory calculations, which contain no zero point vibrational energy, give reasonable estimates of the mean energy partitioning of reactants derived from potential energy barrier release. The timing of bond formation and relative reactivities of different 1,3-dipoles are discussed.

Introduction

For bimolecular reactions, vibrational, rotational, and relative translational energy of reactants can contribute very differently to the efficiency of the reaction.[1−3] These effects were initially explored for atom−diatom reactions, A + BC, which led to a very useful generalization (the Polanyi rules[1]) relating an early or late transition state (TS) to the requirement for translational or vibrational energy of the reactants.

We recently reported the first classical trajectory simulations of 1,3-dipolar cycloadditions, the reactions of three diazonium betaines (nitrous oxide, hydrazoic acid, and diazomethane) with acetylene and ethylene.[3] Among our objectives was an estimate of the relative importance of reactant vibrational, rotational, and translational energy in these six reactions. Another objective was to understand the recently discovered linear correlation between the barriers for the 18 dipolar cycloadditions in Scheme 1 and the energies required to distort the reactants into the TS geometries, $\Delta E_d^{\ddagger}$.[4] This correlation suggests that vibrational excitation of the reactants is an important feature of the mechanism. We found that, in addition to requiring relative translational energy, each cycloaddition requires the excitation of an N−N−Z bending mode of the diazonium betaine to achieve reaction.[3] These bending modes are also the vibrational modes that dominate the TS distortion energy $\Delta E_d^{\ddagger}$.[3]

We have now extended this study to include 12 additional 1,3-dipolar cycloadditions, those of 3 nitrilium betaines and 3 azomethine betaines with ethylene and acetylene. Scheme 1 shows the 18 reactions discussed in this paper. They span a large range of barriers and reaction energies and allow a broader perspective about trends in the requirements for reactant vibration, rotation, and translation in 1,3-dipolar cycloadditions.

Background

Collinear atom−diatom reactions A + BC → AB + C display a simple relationship between the position of the TS (early vs late) and the type of energy (vibration vs relative translation) required to pass through the TS. Figure 1, adapted from Polanyi,[1a] shows the motion of representative trajectories on contour diagrams of two potential energy surfaces; Figure 1a has an early barrier, and Figure 1b has a late barrier. The axes are the asymptotic reaction coordinates, bond lengths r_{AB} and r_{BC}. The reactant energy consists of A/BC relative translation plus BC vibration, and the product energy consists of AB/C relative translation plus AB vibration. The question is which type of reactant energy is required to move through the TS, that is, to move in the direction of the transition vector (the Hessian eigenvector with imaginary frequency) as the TS is approached. With an early barrier, the dominant component of the transition vector is r_{AB}, which corresponds to translation. With a late barrier, the transition vector is mainly r_{BC}, or BC vibration. Note that reactant translation becomes product vibra-

[†] University of California.
[‡] Columbia University.

(1) (a) Polanyi, J. C. *Acc. Chem. Res.* **1972**, *5*, 161. (b) Polanyi, J. C. *Angew. Chem., Int. Ed.* **1987**, *26*, 952.
(2) Barnes, G. L.; Hase, W. L. *Nat. Chem.* **2009**, *1*, 103.
(3) Xu, L.; Doubleday, C. E.; Houk, K. N. *Angew. Chem., Int. Ed.* **2009**, *48*, 2746.
(4) (a) Ess, D. H.; Houk, K. N. *J. Am. Chem. Soc.* **2007**, *129*, 10646–10647. (b) Ess, D. H.; Houk, K. N. *J. Am. Chem. Soc.* **2008**, *130*, 10187.

Scheme 1. 1,3-Dipolar Cycloaddition Reactions of Diazonium Betaines, Nitrilium Betaines, and Azomethine Betaines with Ethylene or Acetylene

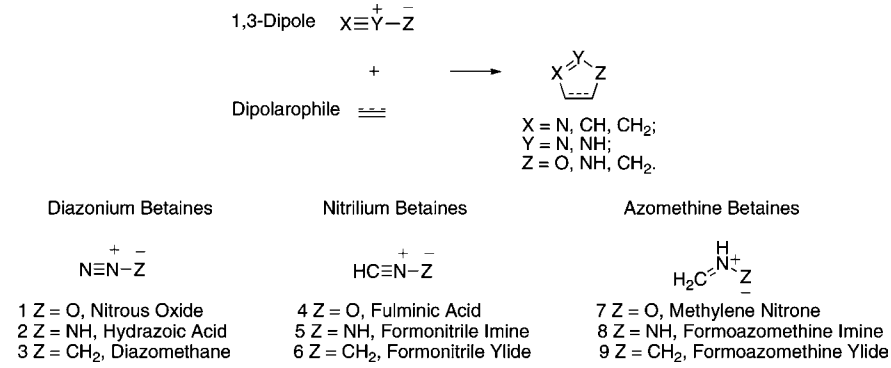

tion with an early barrier, and reactant vibration turns into product translation with a late barrier. Hase et al. have noted that Polanyi's rules need to be generalized for more complex reactions that have many vibrational modes.[5]

Computational Methodology

For the 1,3-dipolar cycloadditions considered here, we assume that conventional transition state theory holds: that the TS dividing surface intersects the saddle point on the potential energy surface, that it is characterized by a Boltzmann distribution of states at a given temperature, and that a trajectory leads to product if and only if it passes once through the TS in the product direction. Since all reactive trajectories must pass through the TS, we take advantage of the time-reversal symmetry of classical mechanics by initializing trajectories at the TS and propagating them in the retro-cycloaddition direction toward reactants to a large separation. This allows the energy distribution to be computed for the subset of reactants that undergo reaction.

Sampling of initial conditions at the TS and integration of trajectories were carried out with a customized version of the Venus[6] dynamics program, in which Gaussian 03[7] was called to compute B3LYP/6-31G* energies and gradients at each step. Two initialization methods were used. First, quasiclassical trajectories (QCT) were initialized by TS normal mode sampling[8−10] with only zero point vibrational energy (ZPE) in each normal mode, 0.6 kcal/mol in the reaction coordinate (the mean value at 298 K), and zero rotational energy. We computed 64−128 QCTs for each reaction.

Second, a single trajectory (ST) was propagated from TS to reactants with no vibrational or rotational energy, not even ZPE, and 0.6 kcal/mol in the reaction coordinate. There is only one ST per reaction. We found that an ST approximates the mean behavior of QCTs for reactions of **1**−**3** with ethylene and acetylene,[3] and the absence of random vibrational noise gives a clearer picture of vibrational energy flow. In recent studies, an ST was used to gain critical insight into a complex thermal rearrangement,[11] and ST energy partitioning into vibration, rotation, and translation has been shown to be in good agreement with the mean values of QCT energy partitioning.[3,12,13] For both QCT and ST, the trajectory was propagated forward and backward in time from the initial point. In the product direction, trajectories were stopped when the new sigma bonds were each less than 1.75 Å.

At the end of the QCT and ST retro-cycloaddition trajectories, the amounts of vibrational, rotational, and relative translational energy in the separated reactants were computed by standard methods.[14] To compute the amount of vibrational energy in each reactant normal mode, we applied the velocity projection method of Raff[15] to the separated reactants at the end of each retro-cycloaddition. After the reactants are separated by 6 Å (closest distance of any pair of atoms in different reactants), the coordinates and momenta are monitored for an additional 200−300 fs. At ca. 1 fs intervals, the instantaneous Cartesian coordinates and velocities of each reactant are transformed to the Eckart frame,[16,17] which minimizes the root-mean-square deviation from the equilibrium geometry in mass-weighted Cartesian coordinates.[17b,18] We used the quaternion method for rotating to the Eckart frame.[17b,19] The Cartesian velocities are then projected onto the normal mode vectors. This allows a set of normal mode kinetic energies to be computed[15] that are averaged over the final 200−300 fs of the trajectory, an interval several times longer than the longest vibrational period. For degenerate bends, the sum of the two energies was averaged. The mean of each mode kinetic energy is multiplied by 2 to get the average mode energy (i.e., equipartition of kinetic and potential energy is assumed).

In a separate calculation, the harmonic contributions of bending modes were calculated from the transition structure. To compute normal mode contributions in a standard reference frame, the distorted reactant geometries in the transition structure were transformed to the Eckart frame.[16−18] The energy ε_i contributed by normal mode i to the total distortion energy is given by $\varepsilon_i = (2\pi c\nu_i q_i)^2/2$, where q_i is the projection of the distortion onto mode i, and ν_i is the frequency of mode i in cm^{-1}. The projection q_i is given by $q_i = \mathbf{L}_i{}^{+}\mathbf{M}^{1/2}(\mathbf{x} - \mathbf{x}_0)$, where $\mathbf{x}$ is the 3Nx1 column vector of Cartesian coordinates of the distorted reactant in the Eckart frame (N = number of atoms), $\mathbf{x}_0$ is the center-of-mass equilibrium geometry, $\mathbf{M}$ is the 3N × 3N diagonal matrix of atomic masses, $\mathbf{L}$ is the matrix of column eigenvectors that diagonalizes the force

(5) Liu, J.; Song, K.; Hase, W. L.; Anderson, S. L. *J. Am. Chem. Soc.* **2004**, *126*, 8602.
(6) Hase, W. L.; Duchovic, R. J.; Hu, X.; Komornicki, A.; Lim, K.; Lu, D.-H.; Peslherbe, G. H.; Swamy, K. N.; Vande Linde, S. R.; Wang, H.; Wolfe, R. J. *VENUS 96. QCPE* **1996**, 671.
(7) Frisch, M. J.; et al. *Gaussian 03*, Revision C.02; Gaussian, Inc.: Wallingford, CT, 2004.
(8) Chapman, S.; Bunker, D. L. *J. Chem. Phys.* **1975**, *62*, 2890.
(9) Peslherbe, G. H.; Wang, H.; Hase, W. L. *Adv. Chem. Phys.* **1999**, *105*, 171.
(10) Doubleday, C.; Bolton, K.; Hase, W. L. *J. Phys. Chem. A* **1998**, *102*, 3648.
(11) Debbart, S. J.; Carpenter, B. K.; Hrovat, D. A.; Borden, W. T. *J. Am. Chem. Soc.* **2002**, *124*, 7896.
(12) (a) Sun, L.; Hase, W. L. *J. Chem. Phys.* **2004**, *121*, 8831. (b) Sun, L.; Park, K.; Song, K.; Setser, D. W.; Hase, W. L. *J. Chem. Phys.* **2006**, *124*, 64313.
(13) Vayner, G.; Addepalli, S. V.; Song, K.; Hase, W. L. *J. Chem. Phys.* **2006**, *125*, 14317.
(14) Porter, R. N.; Raff, L. M. In *Dynamics of Molecular Collisions, Part B*; Miller, W. H., Ed; PLENUM: New York, 1976.
(15) Raff, L. *J. Chem. Phys.* **1988**, *89*, 5680.
(16) Eckart, C. *Phys. Rev.* **1935**, *47*, 552.
(17) (a) Dymarsky, A. Y.; Kudin, K. K. *J. Chem. Phys.* **2005**, *122*, 124103. (b) Kudin, K. K.; Dymarsky, A. Y. *J. Chem. Phys.* **2005**, *122*, 224105.
(18) Jorgensen, F. *Int. J. Quantum Chem.* **1978**, *14*, 55.
(19) http://www.ccl.net/cca/software/SOURCES/FORTRAN/fitest/fitest.shtml.

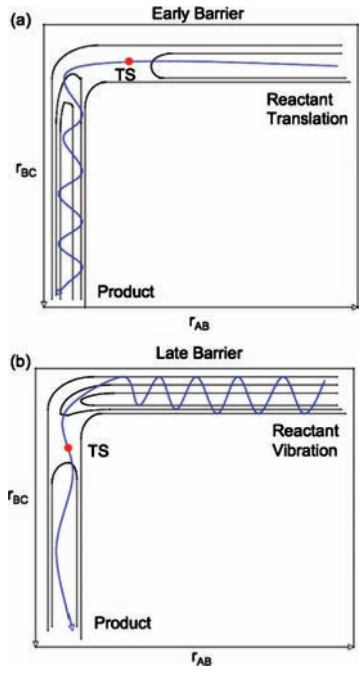

Figure 1. Motion of trajectories on potential energy surfaces a and b for collinear A + BC → AB + C. Axes are the asymptotic reaction coordinates, bond lengths r_{AB} and r_{BC}. (a) Relative translational energy is more effective at promoting reaction with an early barrier. (b) BC vibrational energy is more effective at promoting reaction with a late barrier.

constant matrix, $\mathbf{L}^+$ is the transpose, and $\mathbf{L}_i^+$ is the *i*-th 1 × 3N row eigenvector in $\mathbf{L}^+$.

Results and Discussion

Transition Vector Analysis. The transition structures and transition vectors for reactions of dipoles **1**−**9** with acetylene and with ethylene are shown in Figure 2. The transition vectors are all similar and have several main components: the symmetric stretch of the incipient pair of σ bonds, the dipole bending modes, and a symmetric C_2H_n bending mode. The bending modes that constitute the transition vector lead to the distortions required for reaction to occur. At the TS, these reactant bending modes are part of the reaction coordinate, while at larger distance the IRC (intrinsic reaction coordinate) is mainly translational motion of the reactants (see Figure 1), and the bending modes are orthogonal to the IRC. At some point during the reactants' approach, the IRC must curve, in the 3N-6 dimensional space of internal coordinates, to incorporate the bending modes. This implies that, out of a Boltzmann distribution of reactant vibrational levels, the TS is reached most efficiently by those reactants that already have vibrational excitation in the bending modes that are part of the transition vector.

The transition vectors have nearly equal amplitudes for both forming bonds. Slight deviations are observed for the most unsymmetrical cases (e.g., the reactions of the oxides), but become exactly equal for symmetrical cases (e. g., the reactions of azomethine ylide).

It is useful to have an estimate of the contribution of these various vibrational motions to the TS distortion energy $\Delta E_d^{\ddagger}$, since this energy correlates linearly with the barriers of the reactions in Scheme 1.[4] In the harmonic approximation, the potential energy of distortion of a given reactant at the TS is the sum of contributions from each reactant normal mode. This relationship is accurate only for small displacements from equilibrium, but we find that the sum of harmonic distortion energies deviates from the B3LYP/6-31G* TS distortion energy by only 5−25% in all cases except for the acetylene distortions. This is a small enough error to be qualitatively useful. Table 1 shows the bending mode contributions to $\Delta E_d^{\ddagger}$ for each reactant in the 18 reactions of **1**−**9** + C_2H_n. It gives $\Delta E_d^{\ddagger}$ for each reactant, the contribution to $\Delta E_d^{\ddagger}$ from the sum of the two X−Y−Z bending modes of the dipole, anharmonic corrections for these modes, and frequencies of out-of-plane, in-plane bending of dipoles and symmetric bending of alkenes.

In most cases, the two X−Y−Z bending modes contribute at least half the TS distortion energy $\Delta E_d^{\ddagger}$ of the dipole. This is reasonable, because no other mode of isolated reactants is as efficient in bringing the termini of the reactants together for cyclization. The dominance of $\Delta E_d^{\ddagger}$ by X−Y−Z bending is greatest for **1**−**3** (Table 1), which also have the highest barriers, and diminishes slightly for **4**–**6** (Table 1). For **7**–**9** (Table 1), X−Y−Z bending is important but not dominant. In Table 1, the symmetric bend of C_2H_n is a distant second in importance. For the six reactions of **1**−**3** + C_2H_n, the N−N−Z bending modes account for 64−85% of $\Delta E_d^{\ddagger}$ for the dipole and 45−70% of the total distortion energy, the sum of $\Delta E_d^{\ddagger}$ for dipole and dipolarophile. For **4**−**6**, C−N−Z bending contributes 66−81% of dipole distortion and about half of total distortion. For the planar dipoles **7**−**9**, the in-plane C−N−Z bending contribution is small because **7**−**9** are already bent and the dominant mode is a combination of out-of-plane C−N−Z bending and C−H + Z−H bending (C and Z pyramidalization).

Dynamics Simulations. Having described the importance of vibrational excitation from a static analysis of transition vectors, we turn to the dynamic information that can be obtained from molecular dynamics simulations. Animations of single trajectories (STs) for reactions of all dipoles with acetylene and ethylene can be downloaded at http://www.chem.ucla.edu/~lxu01pku/. Quasiclassical trajectories (QCTs) of reactions of nitrous oxide (**1**), hydrazoic acid (**2**), diazomethane (**3**), fulminic acid (**4**), and methylene nitrone (**7**) with acetylene are also included. Animations include an artificial pause at the transition state geometries; that is the point at which the forward and backward trajectories are started in the simulations.

TS Structures Sampled in QCTs. The TS is not a single saddle point structure, but consists of an infinite number of structures and associated momenta on a hypersurface orthogonal to the reaction coordinate, that divides reactants from products and intersects the reaction coordinate at the saddle point. To choose the initial coordinates and momenta for the trajectories, we used TS normal mode sampling[8−10] to pick a set of structures and momenta on this dividing surface in a manner that approximates a quantum mechanical Boltzmann distribution of vibrational levels. The procedure creates a random distortion of each mode, subject to a quantized Boltzmann distribution.[9] The 64−128 structures chosen by the sampling procedure are, insofar as possible with this small number, an unbiased and representative ensemble of coordinates and momenta that make up the TS dividing surface. Figure 3 shows an overlay of the starting geometries for these calculations, i.e., the structures sampled on the TS dividing surface; each structure represents reactants in the process of colliding to form products. Dipole and dipolarophile bending are the hallmarks of all these geometries. The range of two forming bond lengths in the starting transition structures of QCT is 1.9−2.1 and 2.0−2.3 Å for nitrous oxide (**1**) with acetylene, 2.0−2.3 and 2.0−2.3 Å for hydrazoic acid (**2**) with acetylene, and 2.1−2.4 and 2.2−2.5 Å for diazomethane (**3**) with acetylene. These values are 2.3−2.6

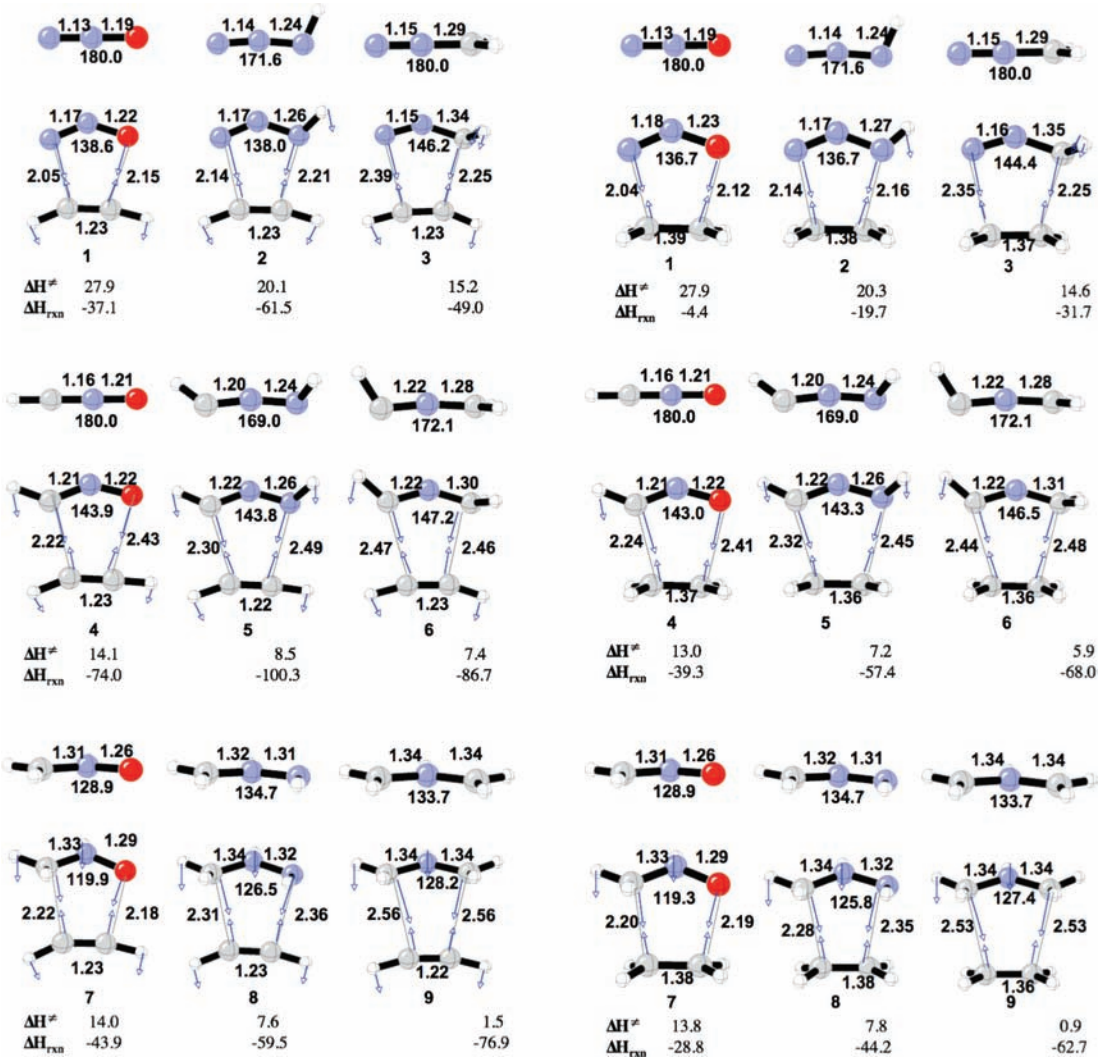

Figure 2. B3LYP/6-31G* geometries of reactants, transition structures and transition vectors of reactions of 1,3-dipoles **1**−**9** with acetylene and ethylene. The bond lengths are given in angstroms and the bond angles are given in degrees. Blue arrows show the direction and relative amplitude of the major movements of atoms that define the transition vectors. CBS-QB3 activation and reaction enthalpies (kcal/mol) at 0 K are given below the transition structures.

Table 1. Comparison of TS Distortion Energies of Reactants with Bending Mode Contributions (in kcal/mol)

	C_2H_4				C_2H_2			
dipole + dipolarophile	$\Delta E_d^{\ddagger a}$	$\epsilon_{bend}{}^b$	$\Delta E_d^{\ddagger}/\Sigma\epsilon_i{}^c$	frequency $(cm^{-1})^d$	$\Delta E_d^{\ddagger a}$	$\epsilon_{bend}{}^b$	$\Delta E_d^{\ddagger}/\Sigma\epsilon_i{}^c$	frequency $(cm^{-1})^d$
1	31.2	26.5	0.91	604, 604	28.2	23.8	0.90	604, 604
Dipolarophile	6.1	3.7	0.90	976	6.5	3.4	0.63	775, 775
2	21.0	11.7	0.93	529, 603	18.7	11.8	0.91	529, 603
Dipolarophile	5.4	3.4	0.90	976	6.3	3.6	0.66	775, 775
3	16.8	10.8	0.84	426, 583	15.1	9.8	0.84	426, 583
Dipolarophile	4.7	3.0	0.92	976	6.8	3.5	0.61	775, 775
4	15.4	10.2	0.85	569, 569	14.4	9.7	0.85	569, 569
Dipolarophile	2.9	1.6	0.94	976	4.0	1.7	0.62	775, 775
5	9.9	8.0	0.94	468, 536	9.3	7.4	0.93	468, 536
Dipolarophile	2.5	1.6	0.95	976	3.8	2.1	0.71	775, 775
6	10.1	7.0	0.86	351, 494	9.5	6.8	0.87	351, 494
Dipolarophile	2.7	1.9	0.95	976	4.9	3.1	0.70	775, 775
7	12.6	7.1	0.75	574, 764	10.9	6.3	0.78	574, 764
Dipolarophile	5.7	3.5	0.89	976	7.5	3.8	0.60	775, 775
8	10.2	5.1	0.79	545, 745	9.0	4.7	0.88	545, 745
Dipolarophile	5.1	3.4	0.91	976	6.4	3.5	0.58	775, 775
9	4.6	2.4	0.83	478, 675	3.6	1.9	0.86	478, 675
Dipolarophile	2.2	1.6	0.94	976	3.9	2.7	0.76	775, 775

[a] TS distortion energy of individual reactants in each of 18 TSs. [b] Contribution to $\Delta E_d^{\ddagger}$ from the sum of in-plane and out-of-plane X–Y–Z bending modes of dipole. Anharmonic corrections have been applied. [c] Anharmonic correction = ratio of $\Delta E_d^{\ddagger}$ to the sum of harmonic mode energies. [d] Frequencies of in-plane and out-of-plane X−Y−Z bends of dipole and symmetric HCCH bend of dipolarophile.

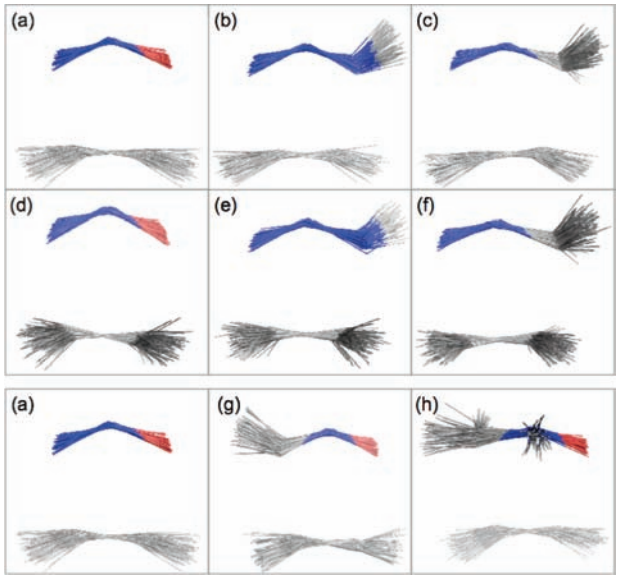

Figure 3. Overlays of 64 starting geometries constituting a Boltzmann distribution in the dividing surface for the quasiclassical trajectories for reactions of 1,3-dipoles diazonium betaines, **1**−**3**, with acetylene (a,b,c) and ethylene (d,e,f), and the oxide 1,3-dipoles **1**, **4**, and **7**, with acetylene (a,g,h).

and 2.1−2.3 Å for fulminic acid (**4**) with acetylene, and 2.1−2.3 and 2.0−2.3 Å for methylene nitrone (**7**) with acetylene. Thus, the range of the geometries on the TS dividing surface is rather wide, 1.9−2.6 Å overall, centering on ∼2.2 Å, a transition state bond length noted earlier to be found for C−C bonds in many hydrocarbon cycloadditions.[20] The saddle point itself is never sampled, but is approximately the centroid of a wide range of geometries, each of which represents a trajectory at the moment it passes through the TS.

ST Energy Partitioning. The single trajectory (ST) has a short history in trajectory studies of organic reactions, but it has been very helpful in several cases. In the study by Carpenter and Borden and co-workers[11] of the 1,2,6-heptatriene rearrangement, an ST played an important role in interpreting the dynamics. Recent studies by Hase and co-workers have shown good agreement between ST energy partitioning and mean QCT energy partitioning for fragmentation of fluoroethane to ethene + HF[12] and for the ozonolysis of propene.[13] We recently reported good agreement between ST and mean QCT energy partitioning for the dipolar cycloadditions of **1-3** with ethylene and acetylene.[3]

Table 2 shows ST energy partitioning for the retro-cycloadditions of dipoles **1**−**9** + C_2H_2, comparing the relative translational, vibrational, and rotational energy in reactants, expressed as the percent of available energy. This is the energy available to reactants in trajectories that start at the TS and proceed toward reactants, and is defined by the initial conditions for STs as

$$E_{\mathrm{avl,ST}} = \Delta E^{\ddagger} + E_{\mathrm{rc}} \qquad (1)$$

where $E_{\mathrm{avl,ST}}$ is the available energies for STs, $\Delta E^{\ddagger}$ is the classical potential energy barrier for the cycloaddition, E_{rc} is the reaction coordinate kinetic energy of 0.6 kcal/mol.

In Table 2, most of the available energy at the TS is supplied by relative translation of reactants. This is consistent with Polanyi's rules.[1] The two new σ bonds are long and weak at the TS (early cycloaddition TS with respect to bond formation). These bonds are important components of the transition vectors (the IRC at the TS), and they rapidly evolve along the retro-cycloaddition IRC into relative translation in the reactant region. As the ST progresses toward reactants, translation receives most of the energy because it quickly becomes the reaction coordinate.

Table 3 shows ST energy partitioning for **1**−**9** + ethylene as the percent of available energy. The trends are similar to ST results for **1**−**9** + acetylene in Table 2, except for a smaller rotational contribution for **4**−**8** + ethylene. Table 2 shows that X−Y−Z dipole bending always dominates the ST vibrational energy of the dipole. (ST vibrational energy is negligible for reactions of **9**.) In all cases, at least half the vibrational energy acquired by the dipole from potential energy barrier release goes into X−Y−Z bending. This is true even when dipole vibration contributes little to the available energy, $E_{\mathrm{avl,ST}}$.

The origin of dipole bending in potential energy barrier release implies that dipole bending excitation is a robust requirement for dipolar cycloadditions that should persist in a variety of conditions. For example, a reviewer suggested that our assumption of a Boltzmann distribution at the TS may not be valid for reactions of small molecules or molecules with rigid functional groups. Most of our reactions are in this category. While the likelihood of a nonstatistical TS distribution is imponderable without specific information, dipole bending would still be important in the nonstatistical case, because bending excitation derives from potential energy barrier release in the retrocycloaddition direction (Tables 2 and 3), and would not be very sensitive to the vibrational distribution at the low vibrational energies considered here (300 K). In the cycloaddition direction, dipole bending combines with translational energy to surmount the barrier, which cannot be done by translation alone.

ST Dynamics. As discussed above, the pair of X−Y−Z dipole bending modes accounts for most of the vibrational energy of the dipole, and dipole bending makes the largest contribution to the correlation of dipolar cycloaddition barriers with TS distortion energy.[3,4] The importance of dipole bending derives from its strong coupling to the IRC in the TS region, and it is useful to see how the dipole acquires bending energy and the reactants receive relative translational energy as the ST moves from the transition state toward reactants.

Figure 4 shows translation and bending occurring in the single trajectories for the reactions of acetylene with **1**, **4**, and **7**, respectively. Each plot shows the trajectory projected onto the 2D space of the dipole bending angle ϕ (defined over 0−360° in the trajectories for **1** and **4** + C_2H_2) and the distance R from the central N atom to the midpoint of the C−C bond. The three reactions of Figure 4 span a range of late to early TSs with respect to X−Y−Z bending, with **1** the latest and **7** the earliest (see Figure 2). All three TSs are early with respect to σ bond formation. Polanyi's rules[1] would predict that (1) a late bending TS requires substantial X–Y–Z dipole bending excitation to pass through the TS, and (2) an early stretching TS requires a large amount of translational energy. Table 2 shows that this is the case, and Figure 4 suggests how this energy is acquired along each retro-cycloaddition ST. From the transition state, initial motion along the transition vector converts the potential energy release into dipole bending and relative translation, the two main components of the transition vector. (The use of nonmass-weighted coordinates makes it appear that the initial motion involves only bending.) The ST soon rebounds from a wall,

(20) Houk, K. N.; Li, Y.; Evanseck, J. D. *Angew. Chem., Int. Ed.* **1992**, *31*, 682.

Table 2. ST Energy Partitioning into Reactant Translation, Vibration, and Rotation for Retro-cycloadditions of **1**−**9** + Acetylene, Expressed As Percent of Available Energy[a]

dipole	$E_{avl,ST}$[b]	%T[c]	$\%V_d$[d]	$\%V_a$[e]	$\%R_d$[f]	$\%R_a$[g]
1	23.9	75	22 (20)	2	1	0
2	17.5	82	15 (15)	2	0	1
3	15.1	78	14 (8)	2	3	3
4	12.7	64	12 (8)	1	8	15
5	8.4	73	7 (7)	0	4	15
6	8.7	72	9 (5)	1	1	17
7	11.7	71	2 (2)	3	5	19
8	7.4	58	1 (1)	2	13	25
9	2.5	94	0 (0)	2	4	0

[a] For a given dipole, %T + %V + %*R* = 100% (±1 due to roundoff). [b] Equation 1, kcal/mol. [c] Percent of $E_{avl,ST}$ partitioned to relative translational energy of reactants. [d] Percent of $E_{avl,ST}$ partitioned to vibrational energy of dipole. (Parentheses: % partitioned to the two X–Y–Z dipole bending vibrations.) [e] Percent partitioned to vibrational energy of acetylene. [f] Percent partitioned to rotational energy of dipole. [g] Percent partitioned to rotational energy of acetylene.

Table 3. ST Energy Partitioning of Retro-cycloaddition Reactions of **1**–**9** + Ethylene, Expressed As Percent of Available Energy, $E_{avl,ST}$ (eq 1)[a]

dipole	$E_{avl,ST}$	%T[b]	$\%V_d$[c]	$\%V_e$[d]	$\%R_d$[e]	$\%R_e$[f]
1	24.1	79	20 (17)	0	1	0
2	17.8	87	13 (12)	0	0	0
3	14.9	85	13 (7)	0	2	1
4	12.0	80	11 (6)	0	4	4
5	7.5	89	4 (4)	0	5	2
6	7.5	92	5 (3)	0	0	3
7	12.0	89	2 (1)	0	3	6
8	7.9	85	1 (1)	0	4	9
9	1.8	68	1 (0)	0	13	17

[a] Sum of percentages in each row = 100 (±1 due to roundoff). [b] Percent of $E_{avl,ST}$ partitioned to relative translational energy of reactants. [c] Percent of $E_{avl,ST}$ partitioned to vibrational energy of dipole. (Parentheses: % partitioned to the two X−Y−Z dipole bending vibrations.) [d] Percent partitioned to vibrational energy of ethylene. [e] Percent partitioned to rotational energy of dipole. [f] Percent partitioned to rotational energy of ethylene.

the outer turning point of the dipole bend. At the same time the IRC, not shown in Figure 4, makes an abrupt right turn toward separation of reactants. As the ST now oscillates down the potential energy barrier toward reactants, potential energy release goes largely into translation.

Figure 4b shows two degenerate bending modes of fulminic acid (**4**), both of which become excited, C−N−O (blue) and H−C−N (red). H−C−N bending has the larger amplitude because of its smaller frequency, 206 vs 569 cm^{-1} for C−N−O bending. However, C−N−O bending receives more energy, 0.97 kcal/mol vs 0.24 for H−C−N bending. This is consistent with C−N−O bending as a requirement for ring formation, while H−C−N bending is required for rehybridization of C at the TS that accompanies bonding. In Figure 4c, the small C−N−O bending amplitude (blue) of **7** reflects the small amount of energy partitioned into this mode, in accord (via Polanyi's rules[1]) with the small bending distortion at the TS (early bending TS). This is expected, since the equilibrium geometry of **7** is already bent. Figure 4c also shows the pyramidalization angle θ_p of the nitrone N atom (turquoise), defined as $\theta_p = \theta_{o\pi} - 90°$, where $\theta_{o\pi}$ is the angle between the π-orbital axis vector (POAV) and the three σ-bonds to N, and the POAV is the vector that makes equal angles to the three σ-bonds at a conjugated atom.[21]

Figure 5 shows translation and bending occurring in the single trajectories for the reactions of acetylene with N_2O (**1**), N_3H (**2**), and CH_2N_2 (**3**), respectively. From Figure 5a to Figure 5c, the bending amplitudes decrease in accord with the bending mode %V of **1**−**3** in Table 4. Among these three dipoles, vibrational excitation is highest in N_2O, followed by N_3H, and lowest in CH_2N_2.

(21) Haddon, R. C. *J. Am. Chem. Soc.* **1997**, *119*, 1797.

Figure 6 shows snapshots from STs of **1**, **4**, and **7** + C_2H_2 at 15 fs intervals. The animations of the full trajectories are shown online: www.chem.ucla.edu/∼lxu01pku. In each reaction, the motion that receives the largest amount of energy from potential energy barrier release is also the most obvious − the rapid separation of reactants. Vibrational energy is harder to spot because of the small amplitudes. For **1** + C_2H_2, whose TS structure is latest with respect to bending, potential energy release gives 4.7 kcal/mol to the N−N−O bend, and 0.5 kcal/mol to the symmetric HCC bend of acetylene, both of which are visible in Figure 6a. In the reaction of **4**, which receives much less vibrational energy than **1**, H−C−N bending motion is identifiable in Figure 6b even though, as noted for Figure 4b, the C−N−O bend receives more energy. The 0.6 kcal/mol total vibrational energy for **7** + C_2H_2 is not apparent in Figure 5c except for C_2H_2 bending.

In contrast to the subtlety of vibrational motions, rotational motion is clearly important in the reactions of **4** and **7** and not for **1**. From Table 2, rotational energy is second in importance only to translation in the STs of **4**-**8**. It is almost twice as large as vibrational energy in **4** + C_2H_2, and nearly five times as large in **7** + C_2H_2. One can also see in Figure 6b and c that the C_2H_2 angular velocity is greater than that of the dipole, and Table 2 confirms that C_2H_2 rotational energy is also greater than the dipole in each case.

Closer scrutiny of Figure 6b and c shows that the C_2H_2 angular velocity increases as the reactants separate. At the same time, the velocity of reactant separation slows, as revealed by the coordinates and momenta. Translation and rotation exchange about 2 kcal/mol in Figure 6b and c during the period of 60−180 fs beyond the TS. This estimate is approximate, because the rotational energies are calculated assuming no interaction

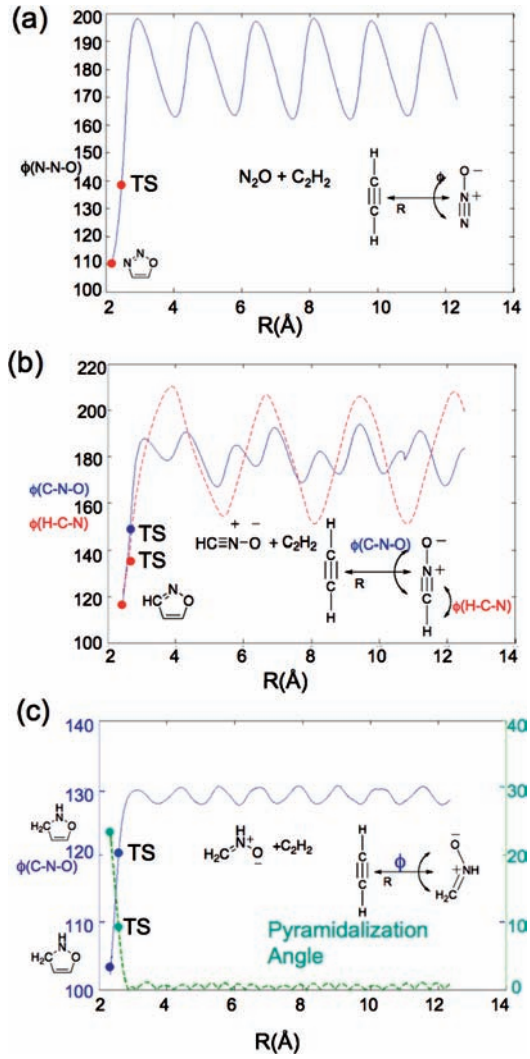

Figure 4. ST trajectory for N_2O (**1**) + C_2H_2, **4** + C_2H_2, and **7** + C_2H_2 at 1 fs intervals. ϕ is the bending angle of the dipole and R is the distance from the central N atom to the midpoint of the C−C bond. Figure 4c includes the pyramidalization angle θ_p at the N atom (turquoise), defined as $\theta_p = \theta_{o\pi} - 90°$, where $\theta_{o\pi}$ is the angle between the π-orbital axis vector (POAV) and the three σ-bonds to N, and POAV is the vector that makes equal angles to the 3 σ-bonds at a conjugated atom.[21] The dipole bending angle scale in Figure 4c is different from the scales in Figure 4a and 4b, since the dipole vibrational amplitude in reaction of dipole **7** with acetylene is extremely small.

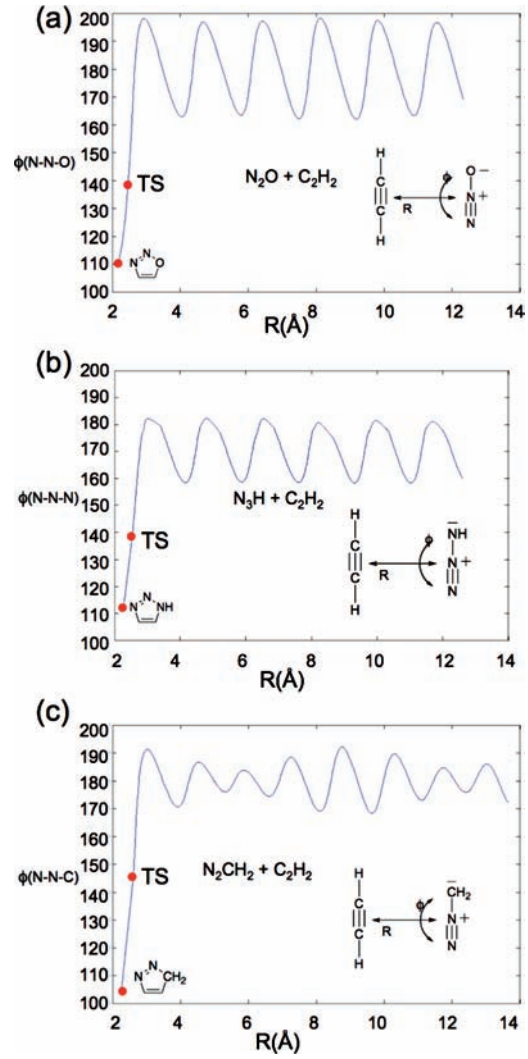

Figure 5. ST trajectory for N_2O (**1**) + C_2H_2, N_3H (**2**) + C_2H_2, and CH_2N_2 (**3**) + C_2H_2 at 1 fs intervals. ϕ is the bending angle of the dipole and R is the distance from the central N atom to the midpoint of the C−C bond.

Table 4. Time Gap between the Formation of the Two New Bonds in STs of Reactions of **1**−**9** with Acetylene and Ethylene[a]

dipole	C_2H_2		C_2H_4	
1	3	10	2	11
2	1	4	1	1
3	6	8	5	7
4	15	13	15	12
5	10	10	7	8
6	1	1	0	0
7	1	1	4	3
8	3	4	4	5
9	0	0	0	0

[a] Time gap is in fs. The first number is for a distance of 1.6 Å, and the second is for 2.0 Å.

between reactants, although clearly an interaction must be present. From the reactant to product direction, the role of rotation is to accelerate the approach of the reactants as collision occurs. Figure 6b and c suggests that the physical interaction responsible for T-R energy transfer is a local interaction of the oxygen with a C−H bond.

Nature of the 1,3-Dipolar Cycloaddition Mechanism. Huisgen established the generality of 1,3-dipolar cycloadditions and clearly showed that these reactions have all the operational signatures of concert: stereospecificity, lack of trappable intermediates, and substituent effects consistent with two-bond processes.[22] Firestone, on the other hand, maintained that a stepwise reaction with a cyclo-diradical might provide an alternative mechanism.[23] In this two-stage mechanism, one σ-bond is formed first, and an unstable diradical intermediate is formed but is short-lived and cyclizes before C−C bond rotation, thus retaining stereochemistry. This is different from a stepwise mechanism involving a longer-lived antidiradical. Scheme 2 contrasts the two mechanisms schematically. Experimental observation of stereospecificity show that a cyclo-diradical cannot have a significant barrier to closure.[24] While it seems clear that no intermediates are formed in most cases, dynamics calculations are necessary to differentiate between a concerted transition state, **10**, and a two-stage process involving

(22) Huisgen, R. *J. Org. Chem.* **1968**, *33*, 2291.
(23) Firestone, R. A. *J. Org. Chem.* **1968**, *33*, 2285.

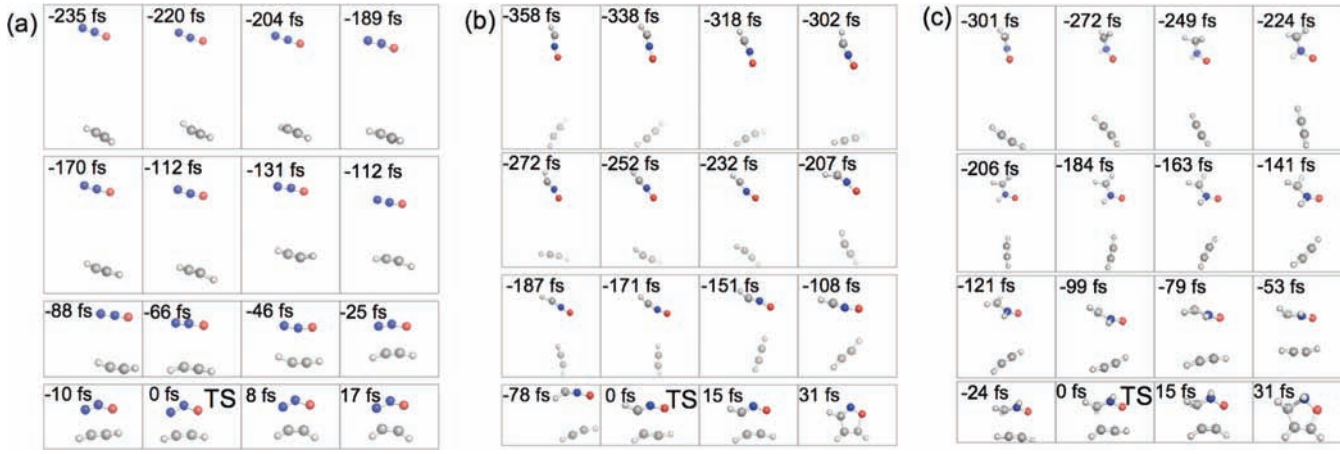

Figure 6. Snapshots at 15 fs intervals of STs of nitrous oxide (**1**), fulminic acid (**4**), and methylene nitrone (**7**) with acetylene. The animations of the full trajectories are shown online: www.chem.ucla.edu/~lxu01pku. The transition structure is indicated for each reaction.

Scheme 2. Concerted and Stepwise Mechanisms for 1,3-Dipolar Cycloadditions

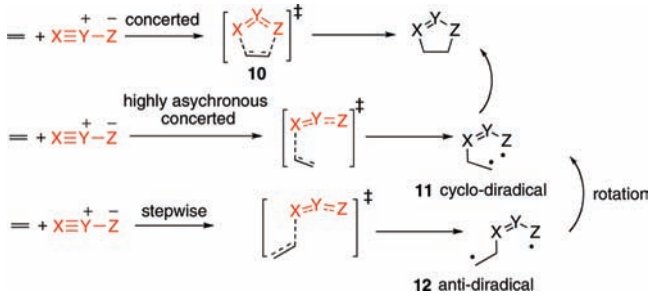

the cyclo-diradical, **11**, that has no significant barrier to form the second bond.

Table 4 shows the time gap (in femtoseconds) between the formation of two bonds in single trajectories for all 18 reactions. Two definitions of bonding are used. The first bond length has decreased to 1.6 Å in single trajectory simulations. The value of 1.6 Å is somewhat longer than that of the product energy minimum, but is still deep in the product well. The second value used is 2.0 Å. This is quite long, in fact near this transition state distance of 2.1−2.6 Å, but still on the product side of the TS. All time gaps in Table 4, from 0 to 13 fs (=1.3×10^{-14} s), are well under the C−C, C−N, or C−O vibrational period of ca. 30 fs. In the distribution of time gaps in QCTs for **1**, **4**, and **7** + C_2H_2, as shown in Figure 7, all time gaps are under 30 fs and the means are in the range of 6−12 fs. These data imply a concerted mechanism in which both bonds are formed within a vibrational period. They are inconsistent with a cyclo-diradical mechanism, since there is no diradical on the surface with a lifetime exceeding that required those atoms to undergo a vibration required for bond formation. These results confirm the concerted nature of the cycloadditions.

The 1,3-dipolar cycloadditions studied here all involve thermal excitation of bending vibrations and collisions in a fashion that brings the termini into a geometry to provide maximum overlap between frontier π orbitals of the two reactants. Collisions involving one center overlap to form longer-lived diradicals in a stepwise mechanism are much higher in energy and are not productive. For those reactions that are stepwise and involving rate-determining formation of a diradical, bending vibrations and distortion energy would be less important than in the concerted processes investigated here.

Lifetime of Reactions. There have been measurements of the lifetimes of intermediates or even transition state of some cycloadditions through femtosecond spectroscopy. According to transition state theory and collision dynamics measurement in the gas phase, reactions involving direct conversion of reactant to product by a single transition state have reaction lifetimes of $\sim 10^{-13}$ s, that is, 100 fs.[25] The time difference between formation of bonds discussed in the previous reaction is much less than this and no bond formation can be considered to occur within the time of a reaction collision of reactants. By contrast, diradicals generated photochemically, but otherwise thought to be identical to diradicals formed in stepwise cycloadditions have much longer lifetimes, 700−1400 fs in the case of tetramethylene and 1,1,4,4-tetramethyltetramethylene.[26] The 1,3-dipolar cycloadditions studied here all exibit the characteristics of concerted process with both bonds formed within the time of a typical vibrational period.

Conclusion

In trajectory calculations for 18 dipolar cycloadditions carried out in the retrocycloaddition direction, we found that potential energy barrier release leads to substantial vibrational excitation in the two X−Y−Z bending modes of the dipole. In the cycloaddition direction, this implies that reactant translational energy alone cannot propel the system through the TS, but must be combined with dipole bending. The importance of translation and dipole bending excitation can be understood by a generalization of Polanyi's Rules[1] to include both types of motions. Translation is important in all 18 cycloadditions because the TSs are early with respect to bond formation. The amount of dipole bending excitation required for reaction depends on the lateness of the TS with respect to dipole bending: diazonium betaines **1**−**3** (late TS, dipole bending required) > nitrilium betaines **4**−**6** > azomethine betaines **7**−**9** (early TS, dipole bending least important).

The previously reported[4] linear correlation between activation barriers and the TS distortion energy of reactants, $\Delta E_d^{\ddagger}$, is closely related to the trends in reactant vibration reported here (Table 1). Since reactant distortion is vibration by definition, $\Delta E_d^{\ddagger}$ can be

(24) Houk, K. N.; Firestone, R. A.; Munchausen, L. L.; Mueller, P. H.; Arison, B. H.; Garcia, L. A. *J. Am. Chem. Soc.* **1985**, *107*, 7227.
(25) Levine, R. D. *in Molecular Reaction Dynamics*; Cambridge University Press: Cambridge, UK, 2005; pp 15−17.
(26) Pedetsen, S.; Herek, J. L.; Zewail, A. H. *Science* **1994**, *266*, 1359.

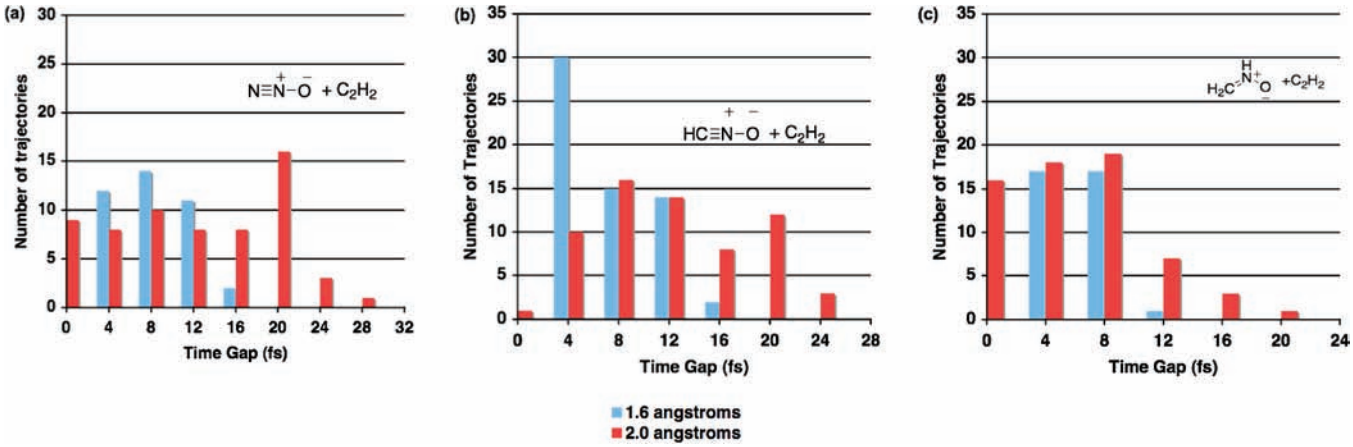

Figure 7. Distribution of time gap of the formation of two bonds in 64 quasi-classical trajectories in reactions of nitrous oxide (**1**), fulminic acid (**4**), and methylene nitrone (**7**) with acetylene. The blue bar is for 1.6 Å and the red bar is for 2.0 Å.

approximated by a sum of harmonic normal mode distortion energies of reactants. The X−Y−Z dipole bending mode energies from this static analysis, based on TS structure alone, parallels the trend in dipole bending mode energies computed by trajectories. The molecular dynamics of these reactions therefore have a close connection to the distortion energy model of reaction barriers[4] (or deformation energy as it is called by Morokuma[27] and activation strain by Bickelhaupt[28]), in which the barrier is analyzed as the sum of reactant distortion energy and intermolecular interaction energy. One difference between trajectories and the distortion energy model is that the dynamical properties of reactants involved in reactive collisions must be obtained by following the full history of each trajectory from TS to reactant, and we note that Bickelhaupt has recently extended his activation strain model to examine strain along the reaction path.[28j] Finally, the timing of bond formation in these reactions confirm the concerted nature of 1,3-dipolar cycloadditions.

Acknowledgment. We are grateful to the National Science Foundation (CHE-0548209, CHE-0616712, and CHE-0910876) for financial and supercomputer support. The computations were performed at the National Center for Supercomputing Applications on Cobalt, TG-CHE050044N, and Abe, TG-CHE090070).

Supporting Information Available: Complete ref 7 and absolute energies and geometries of all the transition structures. This material is available free of charge via the Internet at http://pubs.acs.org.

JA909372F

(27) (a) Kitaura, K.; Morokuma, K. *Int. J. Quantum Chem.* **1976**, *10*, 325. (b) Nagase, S.; Morokuma, K. *J. Am. Chem. Soc.* **1978**, *100*, 1666. (c) Houk, K. N.; Gandour, R. W.; Strozier, R. W.; Rondan, N. G.; Paquette, L. A. *J. Am. Chem. Soc.* **1979**, *101*, 6797. (d) Froese, R. D. J.; Coxon, J. M.; West, S. C.; Morokuma, K. *J. Org. Chem.* **1997**, *62*, 6991. (e) Koga, N.; Ozawa, T.; Morokuma, K. *J. Phys. Org. Chem.* **1990**, *3*, 519. (f) Coxen, J. M.; Grice, S. T.; Maclagan, R. G. A. R.; McDonald, D. Q. *J. Org. Chem.* **1990**, *55*, 3804. (g) Coxon, J. M.; Rroese, R. D. J.; Ganguly, B.; Marchand, A. P.; Morokuma, K. *J. Synnlett* **1999**, *11*, 1681. (h) Avalos, M.; Babiano, R.; Bravo, J. L.; Cintas, P.; Jimnez, J.; Palacios, J.; Silva, M. A. *J. Org. Chem.* **2000**, *65*, 6613. (i) Geetha, K.; Dinadayalane, T. C.; Sastry, G. N. *J. Phys. Org. Chem.* **2003**, *16*, 298. (j) Manoharan, M.; Venuvanalingam, P. *J. Chem. Soc., Perkin Trans. 2* **1997**, 1799. (k) Kavitha, K.; Manoharan, M.; Venuvanalingam, P. *J. Org. Chem.* **2005**, *70*, 2528. (l) Kavitha, K.; Venuvanalingam, P. *Int. J. Quantum Chem.* **2005**, *104*, 67. (m) Blowers, P.; Ford, L.; Masel, R. *J. Phys. Chem. A* **1998**, *102*, 9267.

(28) (a) Bickelhaupt, F. M. *J. Comput. Chem.* **1999**, *20*, 114. (b) Velde, G. T.; Bickelhaupt, F. M.; Baerends, E. J.; Guerra, C. F.; Gisbergen, S. J. A. V.; Snijders, J. G.; Ziegler, T. *J. Comput. Chem.* **2001**, *22*, 931. (c) Diefenbach, A.; Bickelhaupt, F. M. *J. Chem. Phys.* **2001**, *115*, 4030. (d) Diefenbach, A.; Bickelhaupt, F. M. *J. Phys. Chem. A* **2004**, *108*, 8460. (e) Diefenbach, A.; Bickelhaupt, F. M. *J. Organomet. Chem.* **2005**, *690*, 2191. (f) Diefenbach, A.; de Jong, G. T.; Bickelhaupt, F. M. *Mol. Phys.* **2005**, *103*, 995. (g) Diefenbach, A.; de Jong, G. T.; Bickelhaupt, F. M. *J. Chem. Theory Comput.* **2005**, *1*, 286. (h) Stralen, J. N. P. v.; Bickelhaupt, F. M. *Organometallics* **2006**, *25*, 4260. (i) de Jong, G. T.; Visser, R.; Bickelhaupt, F. M. *J. Organomet. Chem.* **2006**, *691*, 4341. (j) de Jong, G. T.; Bickelhaupt, F. M. *Chem. Phys. Chem.* **2007**, *8*, 1170. (k) de Jong, G. T.; Bickelhaupt, F. M. *J. Chem. Theory Comput.* **2007**, *3*, 514.